

Fluid-Structure Interaction Simulation of Aqueous Outflow System in Response to Juxtacanalicular Meshwork Permeability Changes with a Two-Way Coupled Method

Jing Zhang^{1,2,3}, Xiuqing Qian^{1,2}, Haixia Zhang^{1,2} and Zhicheng Liu^{1,2,*}

Abstract: Elevated intraocular pressure appears to have a broader impact on increased resistance to aqueous humor outflow through the conventional aqueous outflow system (AOS). However, there is still no consensus about exact location of the increased outflow resistance of aqueous humor, and the mechanism is not perfect. In addition, it is difficult to accurately obtain hydrodynamic parameters of aqueous humor within the trabecular meshwork outflow pathways based on the current technology. In this paper, a two-way fluid-structure interaction simulation was performed to study the pressure difference and velocity in the superficial trabecular meshwork, juxtacanalicular meshwork (JCM) and Schlemm's canal in response to JCM permeability changes. We obtained the JCM permeability of normal intraocular pressure varied between $1 \times 10^{-15} \text{ m}^2$ and $10 \times 10^{-15} \text{ m}^2$ while permeability of the JCM ranged from $2 \times 10^{-16} \text{ m}^2$ and $3 \times 10^{-16} \text{ m}^2$ under conditions of high intraocular pressure. The study indicated that the fluid dynamics parameters in trabecular meshwork and Schlemm's canal are most significantly affected by the changes of JCM permeability. Moreover, the study demonstrates that the finite element modeling of AOS provides a practical means for studying the outflow dynamics and the biomechanical environment of the AOS.

Keywords: Juxtacanalicular meshwork, fluid-structure interaction, permeability, trabecular meshwork.

1 Introduction

Glaucoma is a series of ocular diseases with the main clinical symptoms of ocular hypertension and can lead to blindness, which is seriously harmful to the quality of humanity life [Kwon, Fingert, Kuehn et al. (2009); Tian, Li and Song (2017)]. The majority of the aqueous humor (AH) (approximately 85%) leaves the eye via the conventional aqueous outflow system (AOS). Aqueous humor moves primarily through the trabecular meshwork (TM), which consists of the uveal meshwork, corneoscleral meshwork, and the juxtacanalicular meshwork (JCM) [Ethier, Johnson and Ruberti

¹ School of Biomedical Engineering, Capital Medical University, Beijing, 100069, China.

² Beijing Key Laboratory of Fundamental Research on Biomechanics in Clinical Application, Capital Medical University, Beijing, 100069, China.

³ College of Medical Imaging, Xuzhou Medical University, Xuzhou, 221004, China.

* Corresponding Author: Zhicheng Liu. Email: zcliu@ccmu.edu.cn.

(2004)], and then flows out Schlemm's canal (SC), enters into the collector channel (CC) and eventually enters into the aqueous vein. Drainage resistance in the AOS is of clinical significance due to the crucial roles it plays in adjusting intraocular pressure (IOP). Clinical evidence suggests that raised IOP is a function of elevated resistance to AH outflow through the AOS. It is postulated that the increase of outflow resistance is provided by the functional changes or structural abnormalities in TM, which leads to ocular hypertension associated with numerous cases of glaucoma [Barany (1954); Johnson (2006); Stamer and Acott (2012)]. Hence, a better understanding of the pathological changes of AH outflow through the AOS can provide valuable information for IOP-lowering treatments of glaucoma patients.

Mice and rats are often used in ophthalmology when investigating the ocular tissues because of their availability, price advantage, and similarities in AOS structures to humans [Chen, Yeh, Liu et al. (2008); Morrison, Fraunfelder, Milne et al. (1995); Reme, Urner and Aeberhard (1983)]. In the human eye, CC is about 22 μm and SC is about 120 μm . And the sizes of CC and SC are smaller in rat eye than in human eye [Hann, Bentley, Vercnocke et al. (2011); Irshad, Mayfield, Zurakowski et al. (2010)]. Therefore, the ability to visualize the structure of AOS at adequate resolution will be of great utility and value. In previous studies, we obtained the TM structures within the AOS in rabbit and rat eyes [Mei, Ren, Xu et al. (2015); Zhang, Ren, Mei et al. (2016)]. In this paper, 2D two-photon microscopy (TPM) images of the rat AOS viewed from the sagittal plane of eye are obtained. Until now, TPM has been considered the most effective tool for imaging the TM, which can acquire subcellular structures in situ without the need for tissue fixation and extrinsic dyes.

The anatomical architecture of AOS tissues is extremely complex and tiny, making experimental testing within the ocular tissues challenging. In this case, imaging and the application of mathematical modeling to compute the structure-function relationship and mechanics is an essential step forward [Liu and Tang (2010); Norman, Flanagan, Sigal et al. (2011); Tang, Yang, Geva et al. (2007); Zuo, Tang, Yang et al. (2015)]. Previous research described several numerical simulations to research the mechanism of AH flow in anterior chamber (AC) [Canning, Greaney, Dewynne et al. (2002); Heys and Barocas (2002); Johnson and Kamm (1983); Scott (1988)]. However, there is little research on the interaction law of the TM outflow pathways and aqueous humor, presumably due to the significant difficulty in obtaining or reconstructing the TM and SC.

In this paper, the 3D models of AOS, including superficial TM, JCM, SC, CC, cornea, iris and lens in the physiological state are obtained as a whole. Furthermore, our research reports, for the first time, 3D reconstruction of the aqueous outflow system was done for TPM-sliced images. And some hydrodynamic parameters of TM, JCM and SC are analyzed under different JCM permeability using a two-way fluid structure interaction (FSI) approach. These parameters provided in our research will be important for further investigation and determination of the primary factor that influenced on outflow resistance. And the work provides an efficient technical means and theoretical basis for the further design of aqueous drainage devices, trabeculectomy and the choice of the best position.

2 Materials and methods

2.1 Tissue preparation

Since the anatomy of the AOS in rats is similar to those of humans, the adult SD (Sprague-Dawley) rats were selected as the experimental animal provided by the animal department of Capital Medical University (IACUC: AEEI-2013-x-123). The eyes (a total of 6 eyeballs) were immediately enucleated after euthanasia and immersed in phosphate buffered saline (PBS; 0.2 g L⁻¹ potassium phosphate monobasic, 8 g L⁻¹ sodium chloride, 2.16 g L⁻¹ sodium phosphate dibasic heptahydrate, pH 7.4) for imaging. The study was approved and monitored by the Institutional Animal Care and Use Committee of the Capital Medical University of Beijing. All experiments were performed in accordance with ethical requirements for Use of Animals.

2.2 Two-photon microscopy imaging

Image capturing was performed using a TPM system at the Research Lab for Biomedical Optics and Molecular Imaging (SIAT, CAS, CHN) [Li, Zheng and Qu (2009); Zheng, Wu, Winter et al. (2017)]. The excitation laser source was provided using a tunable mode-locked Ti: Sapphire laser (Coherent Inc., Santa Clara, CA, USA) emitting a train of approximately 140 fs width pulses at a repetition rate of 80 MHz. The excitation beam (Ti: Sapphire laser) was focused on the sample, and the backscattered signal was collected using by a 20×/1.00 NA water-immersion objective (Olympus Inc.). To eliminate the residual excitation laser, the emitted signal first passed through an FF01-680/SP-25 filter (semrock Inc.), and subsequently, SHG signals were detected using an HQ450/40× (Chroma Inc.) filter. The signal was captured using a photomultiplier tube (PMT) (H742-50, Hamamatsu Photonics Co.). Finally, the z-stack images were gathered and processed using a custom-designed Labview program. And the system was a functional method of that described previously [Mei, Ren, Xu et al. (2015); Zhang, Ren, Mei et al. (2016)]. Fig. 1 provides a schematic diagram showing the image region in rat eye.

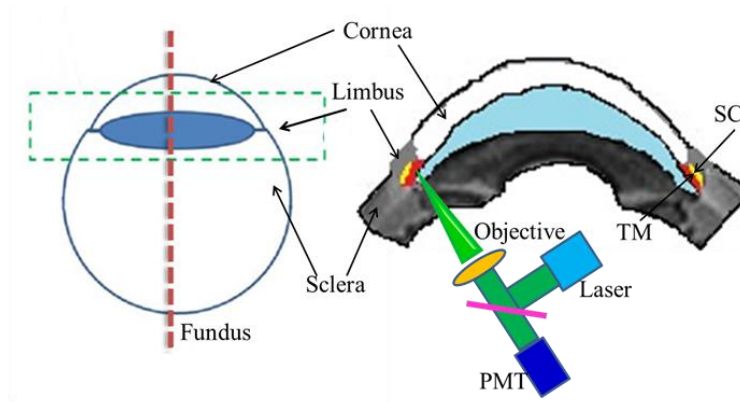


Figure 1: Schematic diagram of the eye and the image system. The laser vertically exposed the surface of the sagittal plane of eye

2.3 3D geometry

In our study, TPM imaging was performed in an enucleated, unfixed, healthy rat eye imaged with the AOS viewed from the sagittal plane of eye. 2D TPM images of the TM outflow pathways viewed from the sagittal plane of eye were obtained, as shown in Fig. 2. In the post-processing step, image enhancement was performed using MATLAB (Mathworks, Natick, MA, USA) to improve contrast and separate the gray range for the region of interest and background. The TM, JCM and SC contours are extracted from the original image through contour extraction, shown in Fig. 3. Firstly, the TM, JCM and SC contours are extracted from the original image in Mimics (Materialise, Leuven, Belgium). And a 3D porous media model of TM outflow pathways was constructed based on the geometric characteristics of the pathways using Solidworks software. In this way, we obtained the fluid model, including JCM, the canal lumen of SC, CC and AH (Fig. 3(b)). Secondly, quite a few morphological parameters of AOS were determined using the experiment measurement integrated with statistical analysis. Furthermore, the 3D models of iris, lens and cornea in the physiological state were obtained. Thirdly, using Boolean operations, we obtained a fluid-structure interaction model of aqueous outflow system. The geometric characteristics of the AOS model are given in the Tab. 1. Finally, a finite element-based FSI simulation was performed to model the AOS using ANSYS (ANSYS Inc., Canonsburg, PA, USA).

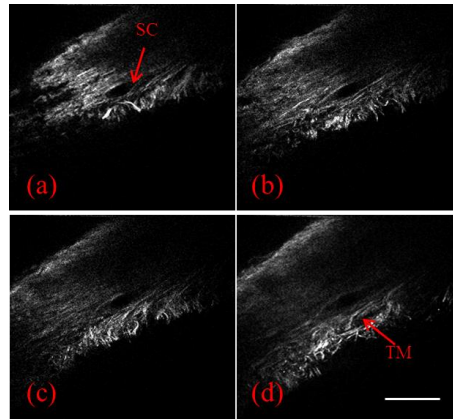


Figure 2: Tomographic sequence images obtained using TPM. (a) and (d) show the SHG images of the TM region at depths of 30 μm and 60 μm . Scale bar=100 μm

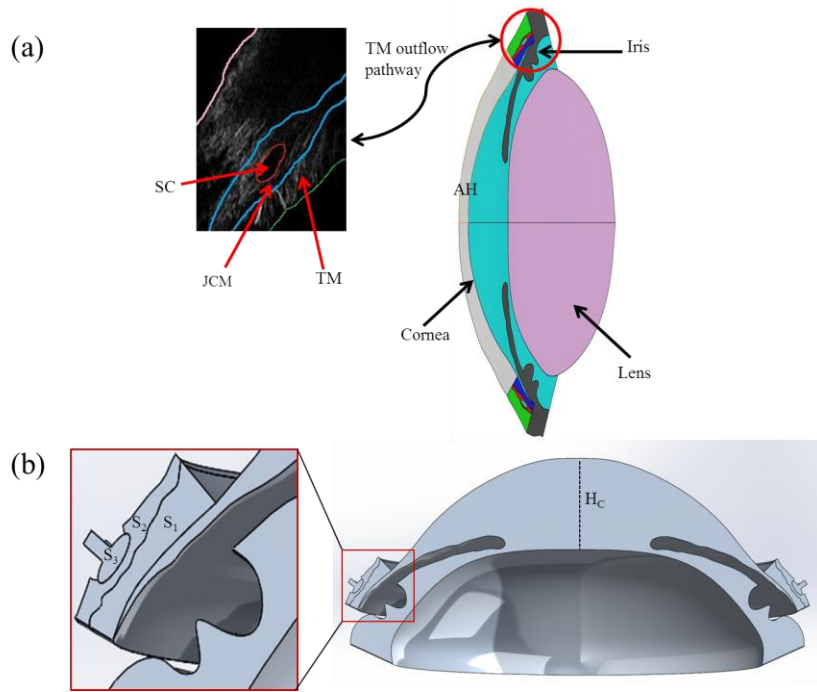


Figure 3: The model assembly. (a) The fluid-structure interaction model of the AOS, and a 2D representation of the idealization model based on TPM image. (b) 3D representation of the fluid model of AOS based on (a) and created by using Solidworks software, and the corresponding structure parameters are shown in Tab. 1

Table 1: Geometric characteristics of the AOS model

Parameter	Value
Cross-sectional area of the TM (S_1)	0.053 mm^2
Cross-sectional area of the JCM (S_2)	0.029 mm^2
Cross-sectional area of the SC and CC (S_3)	0.012 mm^2
The long axes of the SC	0.176 mm
The short axes of the SC	0.057 mm
The diameter of the CC	0.05 mm
Maximum height of chamber H_c	0.95 mm
Angle between cornea and iris	30°

2.4 Boundary conditions

To set up a tractable model of the AOS, the assumption is that the solid model is isotropic and linearly elastic. The inner and outer surfaces of the iris and the corneal endothelium wall were set as FSI surfaces. The temperature difference between the exit of CC (37°C) and the surface of the cornea (35°C) drives the flow of the AH through the AC [Kocak,

Orgul and Flammer (1999)]. In our study, the cornea and iris model were assumed as incompressible material at a Poisson ratio of 0.49 [Heys and Barocas (1999)]. And the contact surfaces between the AH and AOS (cornea, iris and TM outflow pathways) were set as FSI surfaces. An inlet speed of $3 \mu\text{L min}^{-1}$ [Goel, Picciani, Lee et al. (2010)] was applied to the bottom surface of the posterior chamber. The pressure applied to the outlet of CCs was estimated 0.93 kPa to simulate the episcleral venous pressure (EVP). The thesis established a finite element model of aqueous outflow system including the porous media model of layered TM to investigate the effects of TM and JCM permeability on IOP and the pressure difference and velocity in TM and SC. Several values of TM permeability were tested to define the IOP. The boundary conditions and corresponding material properties of AH, iris and cornea used in the model are presented in Fig. 4 and Tab. 2.

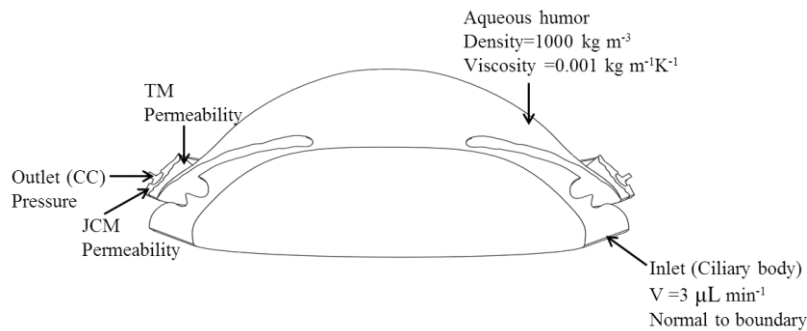


Figure 4: The boundary conditions used in the fluid model

Table 2: Properties of AH, cornea and iris

Properties	Value	Source
Young's modulus of iris	27 kPa	[Heys and Barocas (1999)]
Poisson's ratio of iris	0.49	[Heys and Barocas (1999)]
Young's modulus of cornea	19.1 MPa	[Bryant, Szerenyi, Schmotzer et al. (1994)]
Poisson's ratio of cornea	0.49	[Buzard (1992)]
Volumetric flux	$3 \mu\text{L min}^{-1}$	[Goel, Picciani, Lee et al. (2010)]
Dynamic viscosity	$0.001 \text{ kg m}^{-1} \text{ K}^{-1}$	[Kumar, Acharya, Beuerman et al. (2006)]
Specific heat	$4180 \text{ J kg}^{-1} \text{ K}^{-1}$	[Author and Reviewer (1967)]
Thermal expansion coefficient α	0.0003 K^{-1}	Water
Density	1000 kg m^{-3}	[Kumar, Acharya, Beuerman et al. (2006)]

3 Results

3.1 Permeability

The pressure distribution in the AC, the TM, the JCM, the SC and the CC can be shown by finite element analysis of the AOS model. The pressure difference between the AC and

the EVP determines the outflow resistance of the aqueous humor within TM outflow pathways. The TM was modeled as a porous medium where the permeability parameter was fitted to achieve an appropriate pressure difference between the AC and the CC. The range of TM and JCM permeability under the normal range of IOP fluctuation and pathological IOP fluctuation range can be obtained using finite element analysis. Five groups of TM permeability were analyzed to determine the IOP. The JCM was locked into $1 \times 10^{-16} \text{ m}^2$ and $1 \times 10^{-14} \text{ m}^2$ with an interval of 1×10^{-16} for normal (IOP, less than 21 mmHg) and high IOP simulations (IOP, more than 21 mmHg) referring to previous experimental studies [Mei, Ren, Xu et al. (2015); Zhang, Ren, Mei et al. (2016)]. From Fig. 5, we obtained that the TM permeability of $5 \times 10^{-16} \text{ m}^2$ in group of E, which significantly differed from the TM permeability of $5 \times 10^{-12} \text{ m}^2$ to $5 \times 10^{-15} \text{ m}^2$ in the A to D groups. The JCM permeability with normal IOP ranges from $1 \times 10^{-15} \text{ m}^2$ to $10 \times 10^{-15} \text{ m}^2$, while permeability of the JCM in the AOS model varies between $2 \times 10^{-16} \text{ m}^2$ and $3 \times 10^{-16} \text{ m}^2$ in high IOP condition. The JCM permeability played a greater role in the pressure difference of the TM outflow pathways.

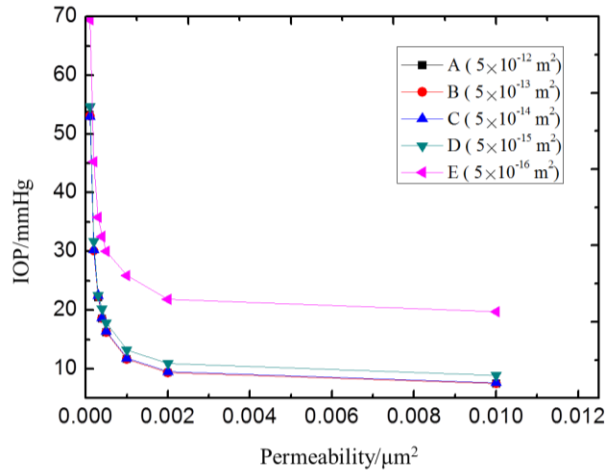


Figure 5: Graph representing the pressure (IOP) in function of the JCM permeability and TM permeability. A-E represents the TM permeability parameter $5 \times 10^{-12} \text{ m}^2$ to $5 \times 10^{-16} \text{ m}^2$ with a ratio of 10^{-1}

3.2 Distributions on trabecular meshwork and schlemm’s canal

A computational model of the AOS for fluid-structure interaction analysis can provide an enlightening explanation of glaucoma where the circulation of AH was impeded. Fig. 4 shows the pressure and velocity distribution results of the TM and SC with a JCM permeability of $2 \times 10^{-4} \mu\text{m}^2$ using the two-way FSI approach. The values (varied between $1 \mu\text{m}^2$ and $8 \times 10^{-4} \mu\text{m}^2$) were set as the JCM permeability in this study to study the flow of aqueous humor through the trabecular meshwork outflow system in response to JCM permeability changes. The simulation results indicated that the pressure and velocity in TM and SC are most significantly affected by the changes of JCM permeability. The pressure distributions on the internal area of TM and the canal lumen of SC are shown in

Fig. 6(a). The pressure magnitude was found to be higher at the AC, TM and JCM regions close to the TM. The highest velocity values in the JCM and TM tissue were calculated to be $1.3 \times 10^{-5} \text{ m s}^{-1}$ and $5.2 \times 10^{-5} \text{ m s}^{-1}$, respectively. In our simulation, high velocities were obtained at the exit of CC, SC, and iris-lens gap. A smaller JCM permeability ($1 \times 10^{-4} \mu\text{m}^2$) obtained a smaller average value of velocity ($1.5 \times 10^{-6} \text{ m s}^{-1}$) in the TM walls, and the JCM region with greater JCM permeability ($2 \times 10^{-4} \mu\text{m}^2$) had bigger average velocity ($2.45 \times 10^{-6} \text{ m s}^{-1}$). There is a progressive decrease in the velocity of the TM and JCM (Fig. 7). Simulated evidence suggested that the outflow resistance was elevated in the smaller permeability of JCM tissue. In comparison with the TM, increasing the JCM permeability in the JCM region had a higher chance of increasing in velocity value of AH. And the simulated results suggested that the outflow resistance was elevated in the smaller permeability of JCM tissue.

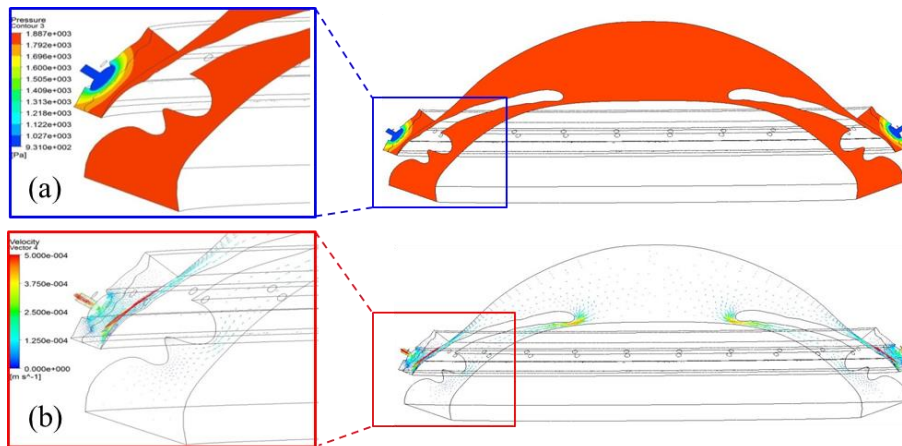


Figure 6: Distributions of AOS model in a rat eye with respective details of the TM and SC (JCM permeability of $2 \times 10^{-4} \mu\text{m}^2$). (a) Contour of pressure. A single coronal cross-section shows the distribution of pressure in different areas of AOS. (b) The velocity vector in AOS

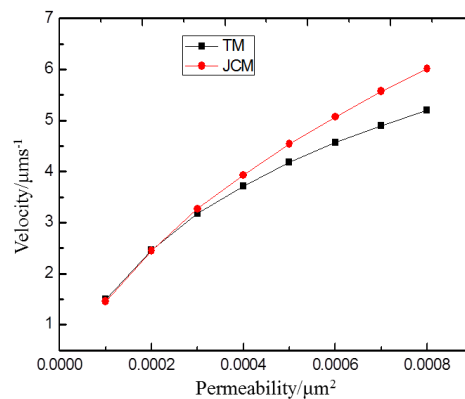


Figure 7: Curves of velocity in TM and JCM with the JCM permeability

3.3 Pressure difference

Fig. 8(a) provides a schematic diagram showing the pressure difference of the TM outflow pathways. There is a progressive increase of the TM pressure difference as a function of the elevated JCM permeability (black curve) (Fig. 8(b)). A higher JCM permeability led to an apparent decrease in the pressure difference of the SC (blue curve) and the JCM (red curve) which leads to the decrease of the AH outflow resistance. Moreover, the findings also demonstrated that the pressure difference was smaller in the TM region than that of the JCM and SC with the same JCM permeability. In comparison with the TM, increasing the JCM permeability in the JCM region had a higher chance of increasing in the AH flow velocity. The simulation result suggests that the outflow resistance within AOS was elevated with the smaller permeability in JCM tissue. Compared to all of the other results, the elevated JCM permeability had a close relationship with the extent of the pressure difference and pressure distribution in AOS, which in turn substantially affects the AH outflow resistance.

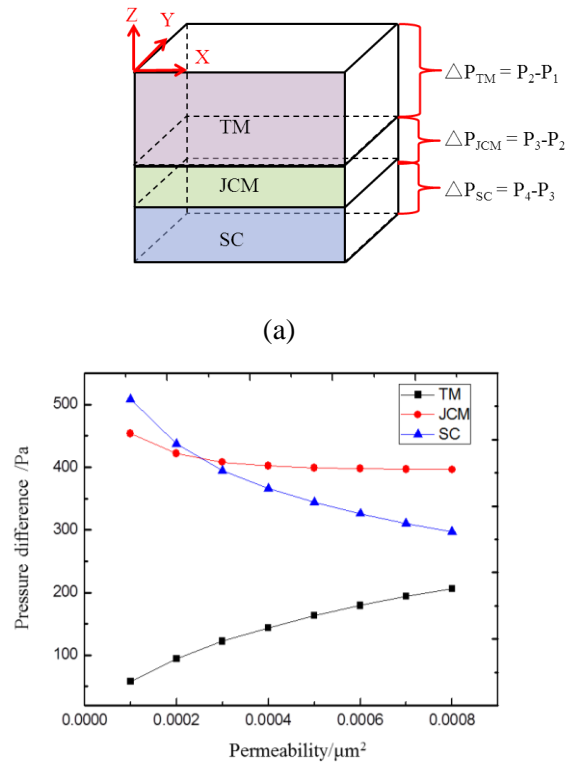


Figure 8: (a) Schematic diagram of the pressure difference of AOS. ΔP_{TM} expresses the difference of pressure between the anterior chamber and the JCM. The negative Z direction corresponds to the direction of flow within TM outflow pathways. (b) Curves of pressure difference in TM, JCM and SC with the JCM permeability

4 Discussion

The resulting pressure difference between the IOP and EVP provides the force for driving the AH out of the eye in the physiological state [Maepea and Bill (1989)]. In our previous study [Mei, Ren, Xu et al. (2015); Zhang, Ren, Mei et al. (2016)], the pressure difference in the AOS is correlated to the permeability of the JCM and can lead to the collapse of AOS tissues, which will contribute to further correlation of AH outflow and IOP. It means that the deformation of TM by raised pressure difference will affect the IOP in turn. It is postulated that the morphology of AH outflow tissues may affect drainage resistance, and there is a potential for an FSI or a two-way coupling between the mechanical behavior of the inner wall of AOS and outflow hydrodynamics [Overby, Stamer and Johnson (2009)]. Murphy et al. [Murphy, Johnson and Alvarado (1992)] obtained that the TM permeability varied between $2 \times 10^{-15} \text{ m}^2$ and $10 \times 10^{-15} \text{ m}^2$ in healthy eyes while permeability ranged from $2.9 \times 10^{-16} \text{ m}^2$ to $3.4 \times 10^{-16} \text{ m}^2$ for glaucoma (eyes). The results of AOS model presented and discussed in this paper is in keeping with these data. Furthermore, the results in this study support the proposal that the JCM of eyes with high IOP may exert a very positive influence part in the change of AH resistance [Johnson (2006); Johnstone (2004); Stamer and Acott (2012)]. The model in this study represented biomechanical coupling of AH and the AOS. Therefore, the relationship between the TM and JCM permeability and the pressure difference and velocity are of the most interest by using a two-way FSI method.

The earliest research on the AH outflow dynamics is to suppose the TM as a single isotropic material that can provide resistance for AH outflow [McEwen (1958)]. Based on histologic sectioning, Villamarina et al. [Villamarin, Roy, Hasballa et al. (2012)] constructed a 3D computational fluid dynamics model of the human eye, which described the TM as a porous material. However, the lack of veracity of the porous medium model of the TM with pores of the same size may limit the accuracy of results from such calculations. We considered that the TM porosity is heterogeneous and performed 3D reconstructions of the AOS from single TPM image of the AOS by imaging the rat eye in situ. The TM was divided into two layers (superficial TM and JCM) in our reconstruction. Meanwhile, we established the 3D models of iris, lens and cornea in normal state. However, there are several issues to be solved in the future. The finite element model will allow for further refinement; for example, material properties of the TM can be assumed to be viscoelastic. Whereas the linearly elastic solutions in this study can serve as a basis for comparison in our future studies of the AOS model in aqueous outflow dynamics with nonlinear materials. Another limitation of our model was that the use of an animal model may not completely reflect the human behaviour. Nevertheless, anatomical characteristics of rat eye are very similar to the human eye [Morrison, Fraunfelder, Milne et al. (1995)]. It is virtually impossible to accurately obtain hydrodynamic parameters of AH within the TM outflow pathways based on the current technology. Our research was to first report the 3D AOS model based on TPM image to analyze the pressure difference of TM and SC in function of the JCM permeability by two-way FSI approach.

In this paper, it is of interest and significance to analyze the pressure difference of TM outflow pathways in response to JCM permeability changes. It had been demonstrated by our simulations that higher permeability in JCM tissue would lead to an increase of flow

speed in TM, including the JCM. Additionally, the outflow resistance is prone to rise proportionally in JCM region and SC with smaller JCM permeability, which increases the venture of developing high IOP in the long run. The results from our AOS modeling research indicated that the changes of permeability in TM tissue may be involved in the elevation of outflow resistance and IOP. Overall, it is necessary to comprehend well that the major factor of the changes of outflow resistance within the AOS in the development of POAG, which will allow for the further improvement in the therapy of glaucoma.

4 Conclusions

The study established an effective finite element model of AOS including the porous media model of layered TM. An algorithm of finite element modeling of the rat TM outflow pathways reveals the importance of TM for JCM permeability, with the potential to assist clinical therapies for glaucoma that seek to steer clear of an abnormal TM. Further studies of glaucoma surgery in the TM involving different parameters could possibly be first tested with the present model. The work presents a valuable means to evaluate the functions and structures of the aqueous outflow pathway for the complicated structure of rat eyes, which can provide evidence for clinical treatment to increase the efflux efficiency of aqueous humor.

Acknowledgement: This work study is financially supported by the National Natural Science Foundation of China (Nos. 31570952, 10802053, 81471702), the Natural Science Foundation of Beijing (No. 3122010). Authors are thankful to Dr. Lu Qingjun for his valuable discussion, an ophthalmologist in Tongren Hospital of Beijing.

References

- Author, G. K. B.; Reviewer, A. D. Y.** (1967): An introduction to fluid mechanics. *Students Quarterly Journal*, vol. 8, no. 29, pp. 37.
- Barany, E. H.** (1954): *In vitro* studies of the resistance to flow through the angle of the anterior chamber. *Acta Societatis Medicorum Upsaliensis*, vol. 59, no. 3-4, pp. 260-276.
- Bryant, M. R.; Szerenyi, K.; Schmotzer, H.; McDonnell, P. J.** (1994): Corneal tensile strength in fully healed radial keratotomy wounds. *Investigative Ophthalmology & Visual Science*, vol. 35, no. 7, pp. 3022-3031.
- Buzard, K. A.** (1992): Introduction to biomechanics of the cornea. *Refractive & Corneal Surgery*, vol. 8, no. 2, pp. 127-138.
- Canning, C. R.; Greaney, M. J.; Dewynne, J. N.; Fitt, A. D.** (2002): Fluid flow in the anterior chamber of a human eye. *IMA Journal of Mathematics Applied in Medicine and Biology*, vol. 19, no. 1, pp. 31-60.
- Chen, C. C.; Yeh, L. K.; Liu, C. Y.; Kao, W. W.; Samples, J. R. et al.** (2008): Morphological differences between the trabecular meshworks of zebrafish and mammals. *Current Eye Research*, vol. 33, no. 1, pp. 59-72.

Ethier, C. R.; Johnson, M.; Ruberti, J. (2004): Ocular biomechanics and biotransport. *Annual Review of Biomedical Engineering*, vol. 6, no. 1, pp. 249-273.

Goel, M.; Picciani, R. G.; Lee, R. K.; Bhattacharya, S. K. (2010): Aqueous humor dynamics: A review. *Open Ophthalmology Journal*, vol. 4, no. 4, pp. 52-59.

Hann, C. R.; Bentley, M. D.; Vercnocke, A.; Ritman, E. L.; Fautsch, M. P. (2011): Imaging the aqueous humor outflow pathway in human eyes by three-dimensional micro-computed tomography (3D micro-CT). *Experimental Eye Research*, vol. 92, no. 2, pp. 104-111.

Heys, J. J.; Barocas, V. H. (2002): A boussinesq model of natural convection in the human eye and the formation of Krukenberg's spindle. *Annals of Biomedical Engineering*, vol. 30, no. 3, pp. 392-401.

Heys, J.; Barocas, V. H. (1999): Mechanical characterization of the bovine iris. *Journal of Biomechanics*, vol. 32, no. 9, pp. 999-1003.

Irshad, F. A.; Mayfield, M. S.; Zurakowski, D.; Ayyala, R. S. (2010): Variation in Schlemm's canal diameter and location by ultrasound biomicroscopy. *Ophthalmology*, vol. 117, no. 5, pp. 916-920.

Johnson, M. (2006): What controls aqueous humour outflow resistance? *Experimental Eye Research*, vol. 82, no. 4, pp. 545-557.

Johnson, M. C.; Kamm, R. D. (1983): The role of Schlemm's canal in aqueous outflow from the human eye. *Investigative Ophthalmology & Visual Science*, vol. 24, no. 3, pp. 320-325.

Johnstone, M. A. (2004): The aqueous outflow system as a mechanical pump-Evidence from examination of tissue and aqueous movement in human and non-human primates. *Journal of Glaucoma*, vol. 13, no. 5, pp. 421-438.

Kocak, I.; Orgul, S.; Flammer, J. (1999): Variability in the measurement of corneal temperature using a noncontact infrared thermometer. *Ophthalmologica*, vol. 213, no. 6, pp. 345-349.

Kumar, S.; Acharya, S.; Beuerman, R.; Palkama, A. (2006): Numerical solution of ocular fluid dynamics in a rabbit eye: Parametric effects. *Annals of Biomedical Engineering*, vol. 34, no. 3, pp. 530-544.

Kwon, Y. H.; Fingert, J. H.; Kuehn, M. H.; Alward, W. L. (2009): Primary open-angle glaucoma. *New England Journal of Medicine*, vol. 360, no. 11, pp. 1113-1124.

Li, D.; Zheng, W.; Qu, J. Y. (2009): Two-photon autofluorescence microscopy of multicolor excitation. *Optics Letters*, vol. 34, no. 2, pp. 202-204.

Liu, B.; Tang, D. (2010): Computer simulations of atherosclerotic plaque growth in coronary arteries. *Molecular & Cellular Biomechanics*, vol. 7, no. 4, pp. 193.

Maepea, O.; Bill, A. (1989): The pressures in the episcleral veins, Schlemm's canal and the trabecular meshwork in monkeys: Effects of changes in intraocular pressure. *Experimental Eye Research*, vol. 49, no. 4, pp. 645-663.

McEwen, W. K. (1958): Application of Poiseuille's law to aqueous outflow. *Archives of Ophthalmology*, vol. 60, no. 2, pp. 290-294.

- Mei, X.; Ren, L.; Xu, Q.; Zheng, W.; Liu, Z. C.** (2015): Effect of persistent high intraocular pressure on microstructure and hydraulic permeability of trabecular meshwork. *Chinese Physics B*, vol. 24, no. 5, pp. 606-613.
- Morrison, J. C.; Fraunfelder, F. W.; Milne, S. T.; Moore, C. G.** (1995): Limbal microvasculature of the rat eye. *Investigative Ophthalmology & Visual Science*, vol. 36, no. 3, pp. 751-756.
- Murphy, C. G.; Johnson, M.; Alvarado, J. A.** (1992): The juxtacanalicular tissue in pigmentary and primary open angle glaucoma: The hydrodynamic role of pigment and other constituents. *Archives of Ophthalmology*, vol. 110, no. 12, pp. 1779-1785.
- Norman, R. E.; Flanagan, J. G.; Sigal, I. A.; Rausch, S. M.; Tertinegg, I. et al.** (2011): Finite element modeling of the human sclera: Influence on optic nerve head biomechanics and connections with glaucoma. *Experimental Eye Research*, vol. 93, no. 1, pp. 4-12.
- Overby, D. R.; Stamer, W. D.; Johnson, M.** (2009): The changing paradigm of outflow resistance generation: Towards synergistic models of the JCT and inner wall endothelium. *Experimental Eye Research*, vol. 88, no. 4, pp. 656-670.
- Reme, C.; Urner, U.; Aeberhard, B.** (1983): The development of the chamber angle in the rat eye. Morphological characteristics of developmental stages. *Graefe's Archive for Clinical and Experimental Ophthalmology*, vol. 220, no. 3, pp. 139-153.
- Scott, J. A.** (1988): A finite element model of heat transport in the human eye. *Physics in Medicine & Biology*, vol. 33, no. 2, pp. 227-241.
- Stamer, W. D.; Acott, T. S.** (2012): Current understanding of conventional outflow dysfunction in glaucoma. *Current Opinion in Ophthalmology*, vol. 23, no. 2, pp. 135-143.
- Tang, D.; Yang, C.; Geva, T.; del Nido, P. J.** (2007): Two-layer passive/active anisotropic FSI models with fiber orientation: MRI-based patient-specific modeling of right ventricular response to pulmonary valve insertion surgery. *Molecular & Cellular Biomechanics*, vol. 4, no. 3, pp. 159-176.
- Tian, H.; Li, L.; Song, F.** (2017): Study on the deformations of the lamina cribrosa during glaucoma. *Acta Biomaterialia*, vol. 55, pp. 340-348.
- Villamarin, A.; Roy, S.; Hasballa, R.; Vardoulis, O.; Reymond, P. et al.** (2012): 3D simulation of the aqueous flow in the human eye. *Medical Engineering & Physics*, vol. 33, no. 10, pp. 1462-1470.
- Yuan, L.; Overby, D. R.; Boussoimmiercalleja, A.; Stamer, W. D.; Ethier, C. R.** (2011): Outflow Physiology of the mouse eye: Pressure dependence and washout. *Investigative Ophthalmology & Visual Science*, vol. 52, no. 3, pp. 1865-1871.
- Zhang, J.; Ren, L.; Mei, X.; Xu, Q.; Zheng, W. et al.** (2016): Microstructure visualization of conventional outflow pathway and finite element modeling analysis of trabecular meshwork. *Biomedical Engineering Online*, vol. 15, no. 2, pp. 323-334.
- Zheng, W.; Wu, Y.; Winter, P.; Fischer, R.; Nogare, D. D. et al.** (2017): Adaptive optics improves multiphoton super-resolution imaging. *Nature Methods*, vol. 14, no. 9, pp. 869-875.

Zuo, H.; Tang, D.; Yang, C.; Gaudette, G.; Billiar, K. L. et al. (2015): 3D fluid-structure interaction canine heart model with patch to quantify mechanical conditions for optimal myocardium stem cell growth and tissue regeneration. *Molecular & Cellular Biomechanics*, vol. 12, no. 2, pp. 67-85.